Supporting Information

Optical Response of Magnetic-Fluorescent Microspheres Used for Force Spectroscopy in the Evanescent Field

Alex Bijamov[1], Fridon Shubitidze[1], Piercen M. Oliver[2], and Dmitri V. Vezenov[2]

[1]Dartmouth College, Thayer School of Engineering, 8000 Cummings Hall, Hanover, NH 03755, USA

[2] Lehigh University, Department of Chemistry, 6 E. Packer Ave., Bethlehem, PA, 18015, USA

dvezenov@lehigh.edu

1. Limitations of the effective medium model. The Maxwell-Garnett model is based on the assumption that an external electric field penetrates conductive inclusions and is uniform within the entire inclusion body. When the inclusion size is greater than either the electromagnetic (EM) field skin depth or the wavelength, however, the corresponding approximations fail, overestimating internal fields. Moreover, previous work[1] showed that, as a general rule of thumb, the size of any particular spherical scatterer should be smaller than 1/10-th of the wavelength – these conditions are fulfilled for cases shown in Table S1 even for the beads made up almost entirely of the nanoparticles discussed. The threshold size of the inclusions can be estimated by setting its diameter equal to the EM field skin depth for lossy dielectrics:

$$\delta_{skin} \sim \frac{2}{\varepsilon'' \varepsilon_0 \omega} \left(\frac{\varepsilon' \varepsilon_0}{\mu \mu_0} \right)^{1/2} \qquad \text{(S1)}$$

where ε' and ε" are, respectively, real and complex parts of material dielectric constants, μ is magnetic permeability, ε_0 and μ_0 are vacuum permittivity and permeability.

Table S1 compares corresponding diameters of inclusions with calculated EM field skin depth for nanoparticle materials at two common laser wavelengths. The results show that the skin depth is much larger than the typical size of inclusions (several to tens of nanometers), thus supporting the applicability of the mixing model.

Table S1. EM properties of magnetite (Fe_3O_4) and quantum dots (core – CdSe, shell – CdS/ZnS)

Material	Diameter	Typical ε_i ($j^2 = -1$)	Skin depth
Excitation wavelength = 410 nm			
Magnetite	8-10 nm	5.64 + j 1.63	0.19 μm
Quantum dots	4-20 nm	7.64 + j 0.18	2.0 μm
Excitation wavelength = 532 nm			
Magnetite	8-10 nm	6.23 + j 0.47	0.9 μm
Quantum dots	4-20 nm	7.44 + j 0.07	7.1 μm

Another possible limitation associated with this model arises from the evanescent character of the fields used. The penetration depth of the evanescent EM field (i.e. E field amplitude decay length) in water resulting from the total internal reflection at the silica-water interface is:

$$\delta_{ev} = \frac{\lambda}{2\pi\left(n_{silica}^2 sin^2(\theta_{inc}) - n_{water}^2\right)^{1/2}} \qquad \text{(S2)}$$

where λ is the incident beam wavelength in vacuum, θ_{inc} is the beam incidence angle in silica, n_{silica} = 1.45 and n_{water}=1.33 are refractive indices of silica support and water. The penetration depths for λ=532 nm are shown in Table S2 for several incident angles. Since the penetration depth of 150-300 nm is at least an order of magnitude greater than the typical size of the inclusions (which are less than 20 nm), the assumption of uniformity of the external field is reasonable. Note, that the penetration depth defined in terms of the characteristic intensity ($\propto|E|^2$) decay length is half of the value for the field amplitude decay length: $\delta_p = \frac{1}{2}\delta_{ev}$.

Table S2. Penetration depths of evanescent EM fields in water at $\lambda = 532$ nm

θ_{inc}	70°	75°	80°	85°
δ_{ev}, nm	286	193	163	150

2. Spectra of component materials. To derive the effective medium properties, it is first necessary to determine the complex dielectric constants of each of its constituent components separately. The major material component of the microspheres, where nanoparticles are embedded, is usually a polymer, such as polystyrene, whose optical indices are readily available in the literature.[2-3] Refractive indices of nanoparticles, especially the dissipative part responsible for light absorption, will be affected by specifics of their size and composition and will deviate significantly from known tabulated values of the bulk materials.[4] Simulations in this paper were based on our own experimental measurements of the extinction coefficient (imaginary part, *k*, of the refractive index $n+jk$) of magnetite nanoparticles (Fe_3O_4) and quantum dots (core – CdSe, shell – CdS/ZnS), while the real parts of the refractive indices (n) were taken from the literature.[5] We used UV-Vis spectroscopy to measure the molar extinction coefficients of the toluene solutions of nanoparticles and converted these values to extinction coefficients of interest, assuming, that the density of the nanoparticles is the same as the density of their bulk analogs: $\rho(CdSe)=5.816$ g/cm^3 and $\rho(Fe_3O_4)=5.175$ g/cm^3.[6] The values of molar extinction coefficients were then linearly extrapolated towards the actual molar densities of Fe_3O_4 and CdSe to obtain the extinction coefficient values of solid materials (Figure S1). These values were then used as inputs for the Maxwell Garnett effective medium approximation.

The experimental values of extinction coefficients point to several important observations: (i) having a large volume fraction of magnetite, although desirable for achieving high pulling forces, may be detrimental to optical detection of the bead position due to significant signal screening that occurs because the extinction coefficient for magnetite is an order of magnitude greater than that for

quantum dots, and (ii) incident illumination in green and red parts of the spectrum is preferable, due to the relative transparency of the magnetite nanoparticles in this range of wavelengths.

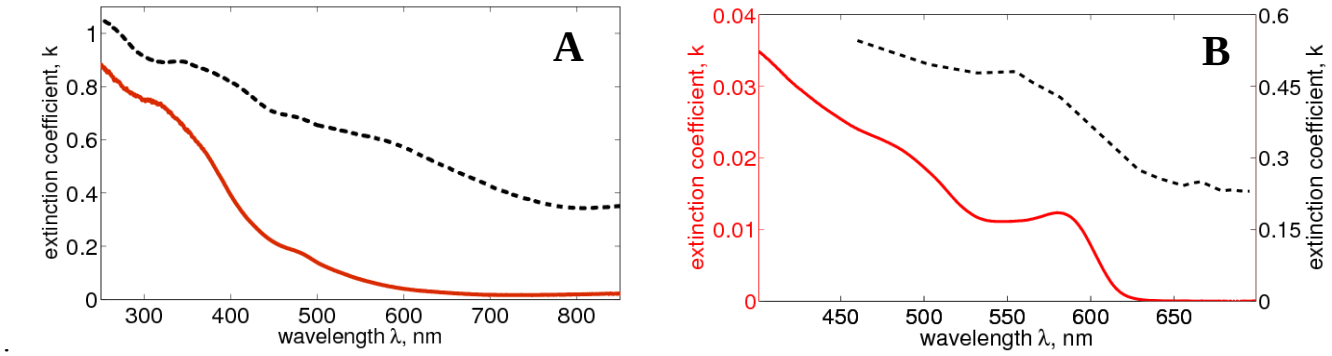

Figure S1. *Extinction coefficient of magnetite Fe_3O_4* ***(A)*** *and CdSe* ***(B)****: measured spectrum (solid, red in color version) of nanoparticles compared to literature data (dotted) for bulk from references [7]* ***(A)*** *and [6]* ***(B)****.*

3. Separation of optical power absorbed in magnetite and quantum dots. The Maxwell-Garnett formula:

$$\varepsilon_{eff} = \varepsilon_b + \frac{3\varepsilon_b \sum_{i=1}^{n} f_i \frac{(\varepsilon_i - \varepsilon_b)}{(\varepsilon_i + 2\varepsilon_b)}}{1 - \sum_{i=1}^{n} f_i \frac{(\varepsilon_i - \varepsilon_b)}{(\varepsilon_i + 2\varepsilon_b)}} \qquad \text{(S3)}$$

describes an effective dielectric constant of composite material having small spherical inclusions doped into a dielectric background. It is based on the assumption that the polarization $\boldsymbol{p_i}$ of any particular sphere depends on its polarizability α_i and Lorentzian field $\boldsymbol{E}_L$ (local field that excites the i^{th} inclusion)[1]:

$$\boldsymbol{p}_i = \alpha_i \boldsymbol{E}_L \qquad \text{(S4)}$$

The polarizability for a sphere with a dielectric permittivity ε_i inside a base medium having permittivity ε_b is well-known:[8]

$$\alpha_i = V_i \frac{3\varepsilon_b(\varepsilon_i - \varepsilon_b)}{\varepsilon_i + 2\varepsilon_b} \qquad \text{(S5)}$$

where V_i is the volume of the i^{th} inclusion. The magnitude of the Lorentzian field depends on the external field $\boldsymbol{E}_e$ and the total dielectric moment induced in the medium[1]:

$$\boldsymbol{E}_L = \boldsymbol{E}_e + \frac{1}{3\varepsilon_b}\boldsymbol{P} = \boldsymbol{E}_e + \frac{1}{3\varepsilon_b}\sum_i n_i \boldsymbol{p}_i \quad \text{(S6)}$$

where the factor of 1/3 is the depolarization factor of the sphere, n_i is the concentration of spherical scatterers of i^{th} type and $\boldsymbol{P}$ is total polarization. Equations S4 and S6 can be combined to yield an expression for the Lorentzian field:

$$\boldsymbol{E}_L = \frac{\boldsymbol{E}_e}{1-\frac{\sum_i n_i \alpha_i}{3\varepsilon_b}} \quad \text{(S7)}$$

Finally, the effective medium parameters are evaluated based on the fact that the effective electric flux density is:

$$\boldsymbol{D} = \varepsilon_{eff}\boldsymbol{E}_e = \varepsilon_b \boldsymbol{E}_e + \sum_i n_i \boldsymbol{p}_i \quad \text{(S8)}$$

Combining Equations S4, S6 and S8 gives:

$$\varepsilon_{eff} = \varepsilon_b + \frac{\sum_i n_i \alpha_i}{1-\frac{\sum_i n_i \alpha_i}{3\varepsilon_b}} \quad \text{(S9)}$$

which yields Maxwell-Garnett formula (Equation S3), when combined with Equation S5. The local electric field, therefore, becomes:

$$\boldsymbol{E}_L = \frac{\boldsymbol{E}_e}{1-\sum_i f_i \frac{\varepsilon_i-\varepsilon_b}{\varepsilon_i+2\varepsilon_b}} \quad \text{(S10)}$$

Once this field is found (which is a direct result of the MAS solution), it can be used to determine the power loss in the inclusion. This field generates electric current in the inclusion, resulting in absorption of optical power. Therefore, the power absorbed by the inclusions of a certain type inside a unit volume is the sum of the powers absorbed in each of the spherical inclusions of this type inside the unit volume:

$$\boldsymbol{P}_i = \frac{V_i n_i}{V}\boldsymbol{j}_i \boldsymbol{E}_L = f_i(\sigma_i \boldsymbol{E}_L)\boldsymbol{E}_L = f_i \sigma_i \boldsymbol{E}_L^2 \quad \text{(S11)}$$

where f_i is volumetric fraction of inclusion of type 'i'. Equation S11 is derived under the same assumptions as the Maxwell-Garnett formula and can, therefore, be used to determine the fraction of power absorbed by each of the components in the mixture. This conclusion is important in our case, because even though the initial evanescent electric field is absorbed by both quantum dots and magnetite inside the sphere, only the fraction of power absorbed by quantum dots is emitted back as a

fluorescent signal. Thus, the emitted power is weighted by both the volumetric fraction of quantum dots and their conductivity, when compared to the entire absorbed power.

4. Simulation of fluorescence. The fluorescence of quantum dots represents spontaneous, rather than induced radiation. This issue needs to be addressed when dealing with the phase distribution of bead volumetric currents. For nanocrystals in a real bead, the phase of the emitted signal is correlated with neither the field exciting it nor the fluorescence of the neighboring nanocrystals. In order to understand the influence of the phase distribution of a set of multiple sources on the total power they emit, we considered a set of 472 electric dipoles, distributed uniformly within a sphere of radius 1.2 μm. Initial magnitudes of the dipole moments were chosen randomly: $\mathrm{A_{i=1\ldots472}}=\mathrm{C}\cdot\left(\mathrm{a_{xi}},\mathrm{a_{yi}},\mathrm{a_{zi}}\right)\cdot\mathrm{e}^{-\mathrm{z_i}/\mathrm{d}}$, where C is a scaling constant, $\mathrm{a_{xi}}$, $\mathrm{a_{yi}}$ and $\mathrm{a_{zi}}$ are random numbers uniformly distributed in the range [-0.5, 0.5] and, finally, the exponential term is included to describe the observed decay of dipole amplitudes with height z (d being the characteristic decay length). With the amplitudes and directions of the sources initially randomized and further fixed, we conducted a series of 1000 simulated measurements of total emitted power, where only the phase of each of the dipoles was being randomized. For the k^{th} realization, the complex amplitude of i^{th} source was set to:

$$A_i = C\cdot\left(a_{xi}\cdot e^{j\varphi_{x,i,k}}, a_{yi}\cdot e^{j\varphi_{y,i,k}}, a_{zi}\cdot e^{j\varphi_{z,i,k}}\right)\cdot e^{-z_i/d} \qquad \text{(S12)}$$

where $\varphi_{x,i,k}$, $\varphi_{y,i,k}$ and $\varphi_{z,i,k}$ are uniformly distributed random numbers in the range $[-\pi,\pi]$. Figure S2 shows a histogram of the total power emitted by this system at 1000 different realizations of the phase distribution among 472 dipoles.

Depending on a specific phase distribution, the total emitted power is different and fluctuates within approximately 2% of the mean value 1.02 with standard deviation of 0.01. When all dipoles are in phase, the total power is 2% less than the mean value. In reality, the signal observed from an individual bead corresponds to an average value from a large number of realizations occurring within a certain time window (corresponding to exposure time of the camera or detector). To simulate the real

experimental conditions, one would have to solve the EM scattering problem multiple times to yield a statistical average of the radiated power; however, this procedure is not time and resource efficient. Instead, we used only a single phase realization to calculate the power radiated by the bead, since we are actually interested in the dependence of the total emitted power on bead composition and location. Namely, since the power fluctuations due to different phase realization for any particular set of parameters (bead diameter, composition, and position) are tightly distributed around the mean, the initial phase value of the field exciting the quantum dots has been preserved (although the source dipoles are not necessarily in phase under these chosen conditions).

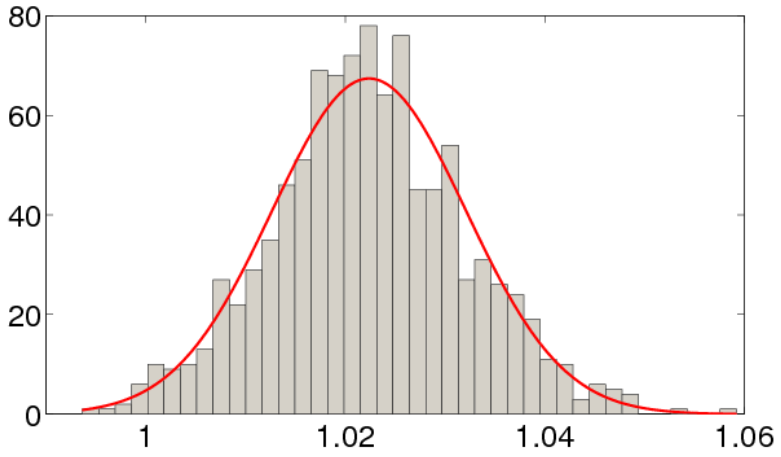

Figure S2. *Distribution of the power emitted by a set of 472 randomly oriented dipoles. Each realization is based on randomizing phases of these dipoles. Power scale is normalized to the total emitted power when all dipoles are in phase. Solid line (red in color version) is a Gaussian fit to the data (mean is 1.02 and standard deviation is 0.01).*

5. Boundary condition matching of MAS solution. The accuracy of the MAS solution in our simulations can be inferred from the mismatch of the boundary conditions (Figure S3). At the absorption stage, the boundary conditions are well satisfied, with mismatch being about 1% for tangential components of electric fields at the boundaries of both the bead and the silica substrate (Figure S3A and S3B). For the fluorescence stage, the relative mismatch is higher than for absorption,

because the amplitude of the field is lower by an order of magnitude, but the mismatch is mostly contained within 5-10 % (Figure S3C and S3D).

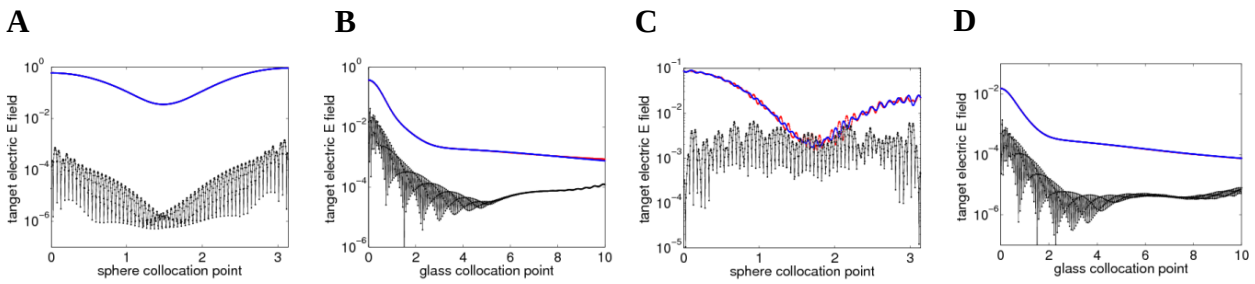

Figure S3. *Boundary conditions mismatch for the simulation of the electric field distribution for a 1 μm diameter bead with high volumetric fractions of composite materials (20% Fe_3O_4, 40% CdSe quantum dots), positioned 60 nm away from the silica-water interface, illuminated by a 532 nm TE-polarized beam incident at an angle of 75°. Blue and red (in color version) smooth curves represent fields evaluated inside and outside of the corresponding boundary and virtually completely overlap. Black curves represent the mismatch (difference) between the two fields.* ***(A)*** *mismatch on the surface of the sphere for the absorption stage;* ***(B)*** *mismatch on the silica surface for the absorption stage;* ***(C)*** *mismatch on a sphere at the fluorescence stage;* ***(D)*** *mismatch on the silica at the fluorescence stage.*

6. Field and power distributions for TM polarization of the incident beam.

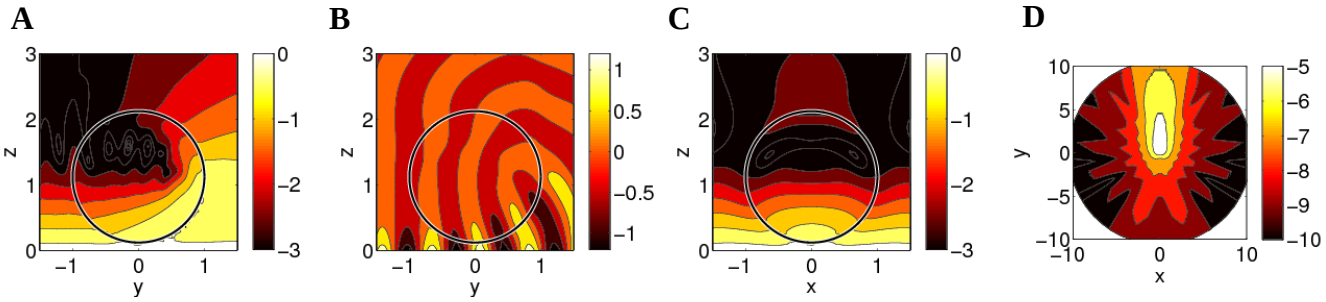

Figure S4. *Electric field, phase, and power distribution for a 1μm diameter bead containing 20% Fe_3O_4 and 5%* ***(A-D)*** *or 40%* ***(E-F)*** *CdSe QDs positioned 60 nm away from the silica-water interface, illuminated by a TM polarized 532 nm beam incident at 75°. All coordinates are in units of bead radius, the color scale in A, C, D, and E is logarithmic, and $|E_{inc}| = 1$ for the incident field.* ***(A)*** *absolute E field distribution in the yz plane;* ***(B)*** *E_x phase distribution in the yz plane;* ***(C)*** *absolute field distribution in the xz plane;* ***(D)*** *distribution of power scattered through silica in the xy plane;* ***(E)*** *absolute E field distribution in the yz plane on a log scale;* ***(F)*** *E_x phase distribution in the yz plane.*

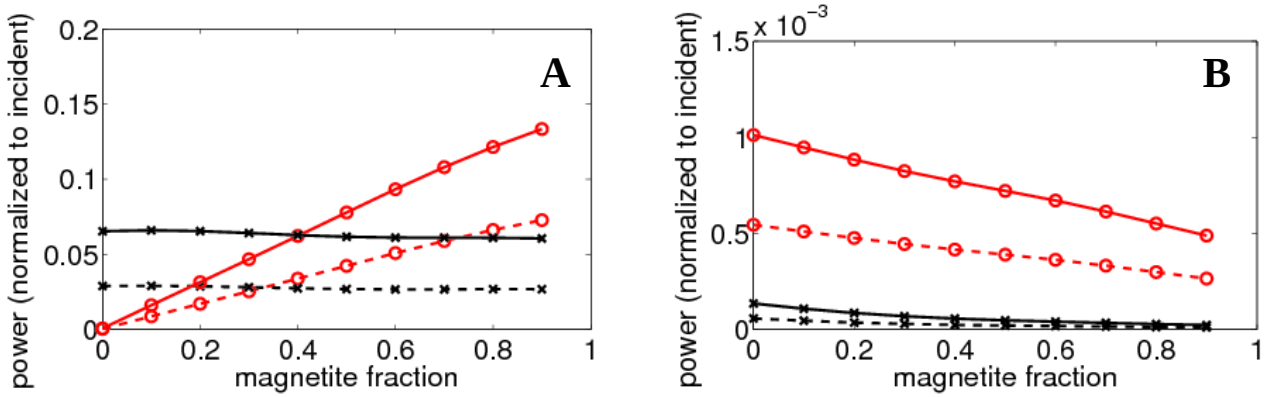

Figure S5. *Power deposited in the bead (o) and scattered through silica (×) during the absorption stage (TM polarization, λ=532 nm)* ***(A)****. Total fluorescent power leaving the bead (o) and detectable fluorescent power (×) (λ=597 nm) as functions of bead magnetite concentration* ***(B)****. (QD volume fraction is constant at 5%, θ=75°, bead diameter is 1.0 μm). Solid and dotted lines correspond to beads positioned 30 nm and 90 nm away from silica. The powers are normalized by the total power available from the incident beam in a silica substrate (for the circular cross-sectional area with a radius equal to the bead radius).*

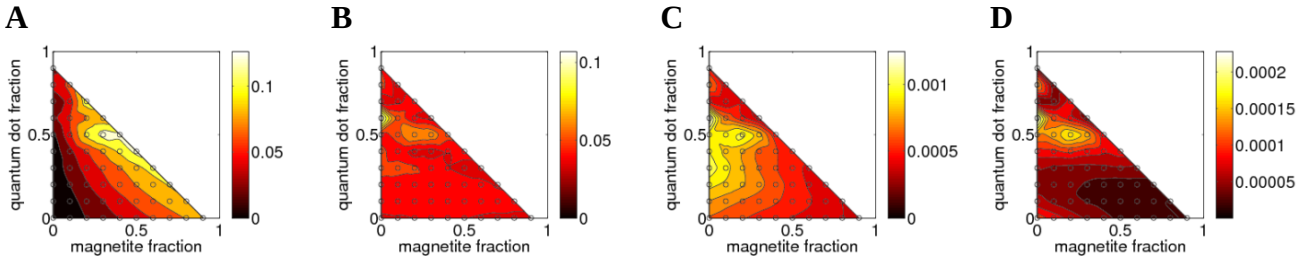

Figure S6. *Power deposited in the sphere* ***(A)*** *and scattered through silica* ***(B)*** *at the absorption stage; power emitted from the sphere* ***(C)*** *and transmitted through silica* ***(D)*** *at the fluorescence stage. All power is plotted as a function of magnetite and QD volume fractions. (TM polarization, θ=75°, bead diameter is 1.0 μm, distance from silica is 60 nm, incident λ=532 nm, fluorescence λ=597 nm).*

References

(1) Sihvola, A. *Subsurface Sens. Tech. Appl.* **2000**, *1*, 393.

(2) Ma, X. Y.; Lu, J. Q.; Brock, R. S.; Jacobs, K. M.; Yang, P.; Hu, X. H. *Physics Med. and Biol.* **2003**, *48*, 4165.

(3) Nikolov, I. D.; Ivanov, C. D. *Appl. Optics* **2000**, *39*, 2067.

(4) Yu, W. W.; Qu, L. H.; Guo, W. Z.; Peng, X. G. *Chem. Mater.* **2003**, *15*, 2854.

(5) Palik, E. D. *J. Opt. Soc. Am. A* **1984**, *1*, 1297.

(6) Roberts, W. L.; Campbell, T. J.; Rapp, G. R. *Encyclopedia of minerals*; 2nd ed.; Van Nostrand Reinhold: New York, 1990.

(7) Huffman, D. R.; Stapp, J. L. *Interstellar Dust and Related Topics. International Astronomical Union Symposium no. 52, State University of New York at Albany, Albany, N.Y., U.S.A. Eds: Greenberg, J. M.; van de Hulst, H. C. Dordrecht, Boston, Reidel* **1973**, 297.

(8) Jackson, J. D. *Classical electrodynamics*; 3rd ed.; Wiley: New York, 1999.